RPNSci

ISSN: 3006-8460 (Online)
3006-8452 (Print)

RESEARCH PROSPECTS IN NATURAL SCIENCES

VOLUME 2
ISSUE 1
2024

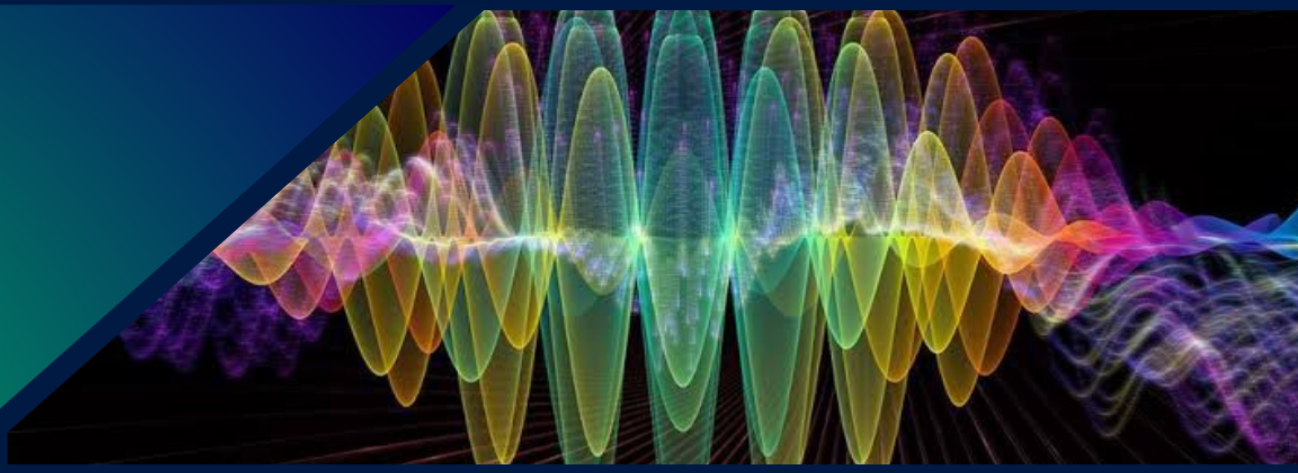

PUBLISHER

GOVERNMENT GRADUATE COLLEGE, TOWNSHIP, LAHORE

RESEARCH PROSPECTS IN NATURAL SCIENCES

Volume 2; issue 1

Publisher: Government Graduate College, Township, LAHORE

Published by Government Graduate College, Township, Lahore.

Publication Data: June 2024

Research Prospects in Natural Sciences: A Research Journal
Printed in Lahore, Pakistan.

Contents

Available online at www.rpnsci.com

ISSN (P): 3006-8452, ISSN (O): 3006-8460

Research Prospects in Natural Sciences Vol. 2, Issue 1, (2024) 1–4

Research Article

A new steroid from chloroform extract of *Tamarix indica*

Sumra Amanat[a,*], Ejaz Ahmed[a], Ahsan Sharif[a], Majda Batool[b], Shazia Amir[b]

[a] *School of Chemistry, University of the Punjab, Lahore 54600, Pakistan*
[b] *Department of chemistry, Government Graduate College, Township, Lahore 54700, Pakistan.*

Abstract

The chloroform soluble fraction of the *Tamarix indica* was used for the first time to purify a new steroid compound as well as four other known compounds. Modern sophisticated techniques such as ^{1}H-NMR, ^{13}C-NMR, EIMS, HREIMS, one dimensional and two-dimensional spectroscopic techniques were used to characterized for structure elucidation of the isolated molecules. The known compounds were recognized as Lupeol **(2)** Stigmasterol **(3)**, Ursolic acid **(4)**, Oleanolic acid **(5)**.

Keywords:
Tamarix indica, Steriods, Terpenoids, ^{1}D NMR and MS techniques, Computational analysis.

1. Introduction

Genus *Tamarix* is the most typical genus of family *Tamaris-caceae* , *Tamarix* is a genus bearing flowering plants of different have about 50-60 species. Mostly species of this genra are present in Africa, Asia and Europe. Height of these plants is maximum eighteen meter and have evergreen broad leaves. Plants with thin branches and grayish green leaves. The genus *Tamarix* have number of species that´s why the family was named *Tamariscaceae*. Seventy-nine type of flowering plants are present in *Tamaris-caceae* (*Tamariscinae*) family, grouped into five genera, which are generally herbs, shrubs and small trees. Phytochemical studies of this genus reveled the presence of following compounds such as sugars, proanthocyanidins alkaloids, quercetin, ellagic acid, flavonols, cyanids, terpenoids, steriods polyphenols, tannin as well as, non-steroids amines and amides, kaempferol accountable for the wide range of medicinal properties.

The speice Tamarix indica is grown in the dry areas of Asia, it is small evergreen. It has hermaphrodite flowers, oblong and rounded petals, pink and white flowers appear as compact-masses at tip of branch alternatively from March to September. It is present mainly in latitude to high altitude especially in Chita hills of Northern areas Indus River Belt, Attock, and Kala in Pakistan. Tamarix indica. has been shown a list of pharmacological activities The methanolicextracts of leafs, barks and also the other major parts of plants revealed cytotoxic, antidiarrheal and antinociceptive activities. Furthermore, the aqueous extracts of bark of this plant were used for aphrodisiacs activities [1–5].

Almost all steroid molecules share a basic structure known as the perhydro-cyclopentanophenanthrene ring system. This consists of four fused rings: three cyclohexane rings (designated as rings A, B, and C) and one cyclopentane ring (designated as ring D), which are arranged in a specific orientation.Despite their structural differences, all steroid molecules share certain properties, such as the ability to bind to specific receptors in the body and influence gene expression [6]. In addition to these established uses, research is ongoing to discover new potential applications for steroids. For example, there is interest in exploring the use of certain steroids as neuroprotective agents in conditions such as Alzheimer's disease, and as anti-aging agents due to their ability to modulate hormone levels and cellular processes. Steroids are also being investigated as potential lead compounds in drug discovery for a wide range of therapeutic areas, including cancer, inflammation, and metabolic disorders [7].

The present work describes the isolation of a new steroid compound and four known compounds from Tamarix indica. The known compound name as Lupeol (2) [8], Stigmasterol (3) [9], Ursolic acid (4) [10], Oleanolic acid (5) [11].

*Corresponding Author:
sumraamanat@gmail.com (Sumra Amanat)

2. Materials and Methods

2.1. General

Silica gel, a commonly used adsorbent material, was used in both thin layer chromatography and column chromatography. Pre-coated preparative plates with silica gel were used to separate and isolate the components of the mixture being studied in TLC. The melting points of the substances were assessed using a Buchi melting point apparatus, which utilizes glass capillaries to contain the sample. Optical rotations, which are a measure of how the sample interacts with polarized light, were measured using a digital polarimeter. Ultraviolet spectra were recorded with the help of Hitachi U-3200 spectrophotometer, while infrared spectra were obtained using an FTIR spectrophotometer. These instruments are used to determine the chemical composition of the substances by analyzing how they interact with different types of electromagnetic radiation.

The ^{1}H-NMR spectra were obtained using TMS (tetramethylsilane) as a reference in $CDCl_3$ (deuterated chloroform), while ^{13}C-NMR spectra were obtained at specific frequencies in $CDCl_3$. Nuclear Magnetic Resonance (NMR) spectroscopy is used for the identification of individual atoms in the substance being studied.

To obtain precise mass measurements, mass spectrometry was used, with glycerol and thioglycerol as matrices. Cesium iodide (CsI) was used as an internal standard. Mass spectrometry is a technique that allows for the determination of mass of individual atoms or molecules in a sample. Ceric Sulphate reagent was used to visualize the spots on TLC plates through spraying. This reagent consists of Ceric sulphate, trichloroacetic acid, and conc. H_2SO_4, and reacts with the substances on TLC plates to produce visible spots. Finally, all chemicals and enzymes used in the determination of enzyme inhibition activities, including antimicrobial, lipoxygenase, and Brine shrimp tests, were sourced from Sigma, a well-known supplier of laboratory chemicals and equipment. These tests were likely performed to determine the efficacy of various substances as inhibitors of certain enzymes or as antimicrobial agents.

2.1.1. Plant Material

Tamarix indica was collected in May from Attock and recognized by Botany Department, University of Karachi where voucher specimen (H.No : 68370) have been kept in herbarium center.

2.1.2. Isolation

6 Kg whole dried powder form plant was used, it refluxed with ethanol (95 %). The crude extract (0.5 Kg) was obtained by evaporating under reduced pressure, separated between *n*-hexane, chloroform, ethyl acetate, *n*-butanol, and water soluble fractions. The chloroform soluble part (150g) were recolumn chromatographed and eluting with *n*-hexane- chloroform and chloroform-methanol, 11 major fractions obtained labeled as T^1-T^{11} (T=*Tamarix*).

The fraction T^5 (*n*-hexane-chloroform, 5:5) revealed many spots on silica gel TLC after re-chromatographed over PTLC using n-hexane-acetone (8.0:2.0) the solvent system gave compound **5** (8 mg). The fraction T^7 (n-hexane-chloroform, 4:6) exhibited five spots on TLC, re-chromatographed over silica gel column chromatography, eluting with *n*-hexane-ethyl acetate (6.0-3.0) solvent system afforded compound **1** (28 mg) and 4(20mg). The fraction T^{10} (*n*-hexane-chloroform, 2:8) showed six major spots on TLC were rechromatographed and finally Preparative silica gel TLC system *n*-hexane-acetone (5.5 : 4.5) to give compound **2** (13 mg) and compound **3** (18 mg).

*2.1.3. (3β, 22E)-stigmasta-7, 9(11), 22-trien-3-yl dodecanoate (new compound) **(1)***

The compound is a colorless, amorphous solid with a specific rotation of -23.0 (c = 1.0, MeOH) at 22°C. Its FT-IR spectrum shows characteristic peaks at 1715 cm^{-1} (carbonyl moiety), 1650-1600 cm^{-1} (olefin group), and 1227 cm^{-1} (C−O). The ^{1}H-NMR spectrum (recorded at 500 MHz in $CDCl_3$) exhibits signals at δ 1.21-1.25 (m, 18H, H-3´-11´), 2.34 (t, 2H, J = 7.5 Hz, H-2´), 0.85 (t, 3H, J = 6.5 Hz, H-12´), 4.24 (dt, 1H, J = 10.8, 8.9 Hz, H-3), 5.35 (t, 1H, J = 7.8 Hz, H-11), 5.13 (dd, 1H, J = 15.2, 7.6 Hz, H-22), 5.03 (dd, 1H, J = 15.1, 7.3 Hz, H-23), 0.98 (s, 3H, Me-19), 6.04 (t, 1H, J = 7.3 Hz, H-7), 0.5 (s, 3H, Me-18), 0.82 (d, 3H, J= 6.4 Hz, Me-21), 0.81 (d, 3H, J = 6.2 Hz, Me-27), 0.52 (t, 3H, J = 7.2 Hz, Me-29), 0.86 (d, 3H, J = 6.2 Hz, Me-26)

The ^{13}C-NMR spectrum (recorded at 125 MHz in $CDCl_3$) shows signals at δ 174.7 (C-1´), 21.1 (C-2´), 28.1-29.2 (C-3´-C-11´), 54.3 (C-12´), 34.5 (C-1), 27.1 (C-2), 72.9 (C-3), 33.1 (C-4), 39.2 (C-5), 29.5 (C-6), 117.5 (C-7), 136.3 (C-8), 144.4 (C-9), 32.5 (C-10), 118.2 (C-11), 41.8 (C-12), 40.4 (C-13), 50.7 (C-14), 23.2 (C-15), 27.7 (C-16), 54.2 (C-17), 11.6 (C-18), 19.1 (C-19), 37.2 (C-20), 18.4 (C-21), 33.4 (C-22), 26.3 (C-23), 45.6 (C-24), 28.7 (C-25), 18.2 (C-26), 19.7 (C-27), 23.1 (C-28), and 12.2 (C-29)

3. Results and Discussion

By subjecting the chloroform-soluble fraction of the *T. indica* plant to column chromatography, a total of five compounds were separated and identified, including four previously known ones and a newly discovered compound. It (1) was purified colorless amorphous solid compound from chloroform soluble extract of plant. **Salkowski and Lieberman Burchard** reaction showed steroidal nature of compound. In HREIMS data molecular ion peak appeared at m/z 592.5201, determined molecular formula (Calculated for $C_{41}H_{68}O_2$, 592.5254) and exhibited eight degrees of unsaturation in compound.

The IR (ν_{max} cm^{-1}) spectral data displayed peaks at 1715 cm^{-1}, 1227 cm^{-1} and 1650 cm^{-1} indicated carbonyl carbon, ester linkage and olefinic moiety respectively. EIMS data exhibited a major fragment peak at m/z 452 ($C_{31}H_{49}O_2$) after the loss of side chain, peak at m/z 140 ($C_{10}H_{19}$) is distinctive feature of steroid molecules. Another major peak appeared at m/z 548 [M−CO_2] showed presence of two oxygen atoms in molecule. Presence of two olefinic moieties in steroid ring B and C, C=O. is indicated by Peak appeared at m/z 411 ($C_{28}H_{44}O_2$) after fission of D ring.

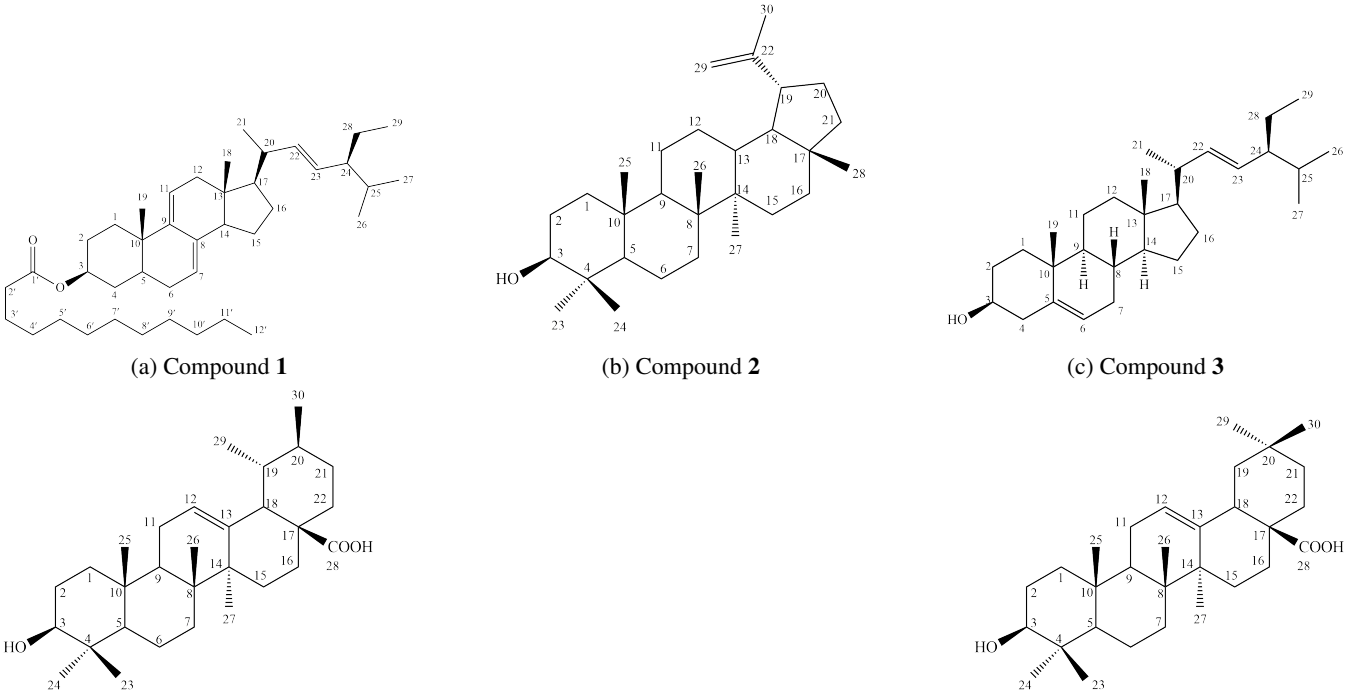

(a) Compound **1** (b) Compound **2** (c) Compound **3**

(d) Compound **4** (e) Compound **5**

Figure 1: Structures of compounds **1-5**

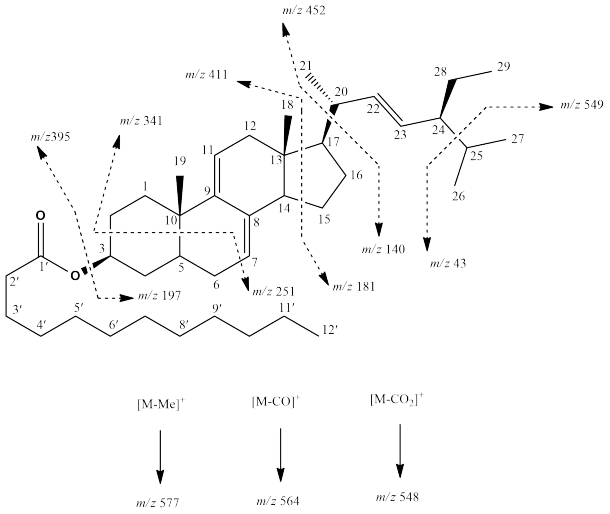

Figure 2: Important mass fragmentation of compound **1**

The presence of a steroid was indicated in the ^{1}H-NMR spectrum by downfield signals at δ 4.24 (H-3), δ 6.04 (H-7), and 5.35 (H-11), which revealed an oxymethine functional group connected to four neighboring proton atoms, a tri-substituted C=C bond, and Δ7,9(11) unsaturation, respectively. Signals at δ 5.13 and 5.03 showed a 1,2-disubstituted olefinic unsaturated bond. Upfield signals at δ 0.98 and 0.51 were due to an angular methyl group and a steroidal methyl group at secondary carbon atoms, respectively. Doublets appeared at δ 0.82, 0.86, and 0.81, indicating a steroidal methyl group. A triplet signal at δ 0.85 showed a dodecanoyl moiety, and a multiplet signal between δ 1.21-1.25 indicated nine methyl groups. A signal at δ 2.34 indicated the presence of a methylene along with a carbonyl carbon. In the ^{13}C-NMR spectrum, the presence of an ester linkage (C=O) was indicated by a signal at δ174.7. The compound structure was further interpreted using proton-proton COSY and HMBC correlation.

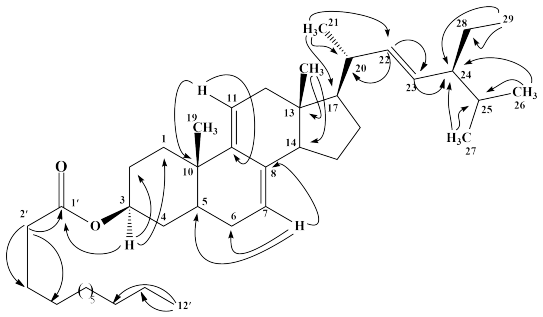

Figure 3: Important HMBC correlation in compound **1**

The HMBC data showed a signal at δ 4.61, indicating the oxymethine proton of C-3, which is a carbon atom with a hydroxyl (-OH) group attached to it. The J2 correlation observed with C-2(δ 27.1) and C-4(δ 33.3) indicates that these carbon atoms are adjacent to C-3, while the J3 correlations with C-1' signal at δ 170.1, C-1, at δ 34.4 and C-5 at δ 39.3 indicate that they are also connected to other parts of the molecule. The β and equatorial configuration of the acetate group is also noted, which is a typical feature of steroids. Olefinic proton at C-7, which is a carbon atom with a double bond (=) attached to it.

The J2 correlation with C-9 at δ 144.5 and C-12 at δ 41.9 indicates that these carbon atoms are adjacent to C-7, while the J3 correlations with C-8 at δ 136.2, C-10 at δ 32.6, and C-13 at δ 40.5 indicate that they are also connected to other parts of the molecule. The equatorial 3β configuration of the molecule is also noted, which indicates the orientation of the functional groups attached to the carbon atoms. All these correlations was confirmed position of the olefin moieties at C-7 and C-9 in the molecule and equatorial 3β configuration

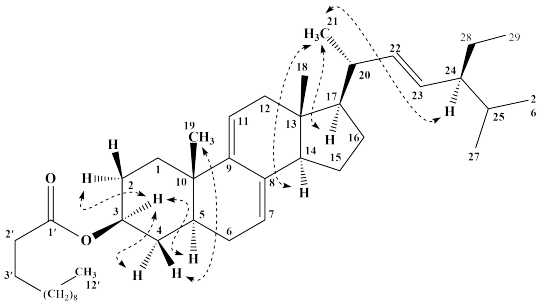

Figure 4: Important NOESY correlation in compound **1**

The compound 1 produced a methyl dodecanoate and a free alcohol when subjected to basic hydrolysis. In HR EI-MS the alcoholic moiety showed peak at m/z 410.5010 for molecular formula $C_{29}H_{48}O$ (Calcd. 410.3548), showing m.p 160 - 161° C, was identified as stigmasta-7, 9 (11), 22- triene-3-ol [12, 13]. The indication of methyl dodecanoate moiety in compound 1 was determined by following comparison those data reported in the literature, by relative TLC comparison of compound with an authentic liquid sample, by boiling point which showed at 260-2614°C and by ^{1}H-NMR and IR spectral data [14]. The compound 1 was identified as (3β, 22E)-stigmasta-7, 9 (11), 22-trien-3-yl dodecanoate in all of these investigations

4. Conclusion

Comparison of spectral and physical data of known compounds (Figure 1) with literature these compound were recognized as Lupeol **(2)** Stigmasterol **(3)** Ursolic acid **(4)** , Oleanolic acid **(5)**

References

[1] N. Al-Jaber, L. Allehaib, The pharmacological activity of some tamaricaceae plants, Natural Products Chemistry & Research 5 (3) (2017) 1–6.

[2] M. J. Christenhusz, J. W. Byng, The number of known plants species in the world and its annual increase, Phytotaxa 261 (3) (2016) 201–217.

[3] R. Ksouri, H. Falleh, W. Megdiche, N. Trabelsi, B. Mhamdi, K. Chaieb, A. Bakrouf, C. Magné, C. Abdelly, Antioxidant and antimicrobial activities of the edible medicinal halophyte tamarix gallica l. and related polyphenolic constituents, Food and Chemical toxicology 47 (8) (2009) 2083–2091.

[4] M. Rahman, E. Haque, M. Hasanuzzaman, I. Shahid, Antinociceptive, antiinflammatory and antibacterial properties of tamarix indica roots, International Journal of Pharmacology 7 (4) (2011) 527–531.

[5] S. Srivastava, G. Choudhary, Pharmacological activity of tamarix troupii: A short review, Sch. Acad. J. Pharm 3 (5) (2014) 363–365.

[6] G. Marwat, A. K. I. HUSSAIN, S. KALSOOM, A review on naturally occurring steroids, Jour. Chem. Soc. Pak. Vol 27 (4).

[7] A. Sultan, A. R. Raza, Steroids: a diverse class of secondary metabolites, Med chem 5 (7) (2015) 310–317.

[8] D. Burns, W. F. Reynolds, G. Buchanan, P. B. Reese, R. G. Enriquez, Assignment of 1h and 13c spectra and investigation of hindered side-chain rotation in lupeol derivatives, Magnetic Resonance in Chemistry 38 (7) (2000) 488–493.

[9] I. Rubinstein, L. J. Goad, A. Clague, L. J. Mulheirn, The 220 mhz nmr spectra of phytosterols, Phytochemistry 15 (1) (1976) 195–200.

[10] J. S. Alves, J. C. de Castro, M. O. Freire, E. V. L. da Cunha, J. M. Barbosa-Filho, M. S. de Silva, Complete assignment of the 1h and 13c nmr spectra of four triterpenes of the ursane, artane, lupane and friedelane groups, Magnetic Resonance in Chemistry 38 (3) (2000) 201–206.

[11] J. P. A. Goossens, Oleanolic acid, Phytochemistry 77 (2012) 10–15.

[12] E. Ahmed, S. A. Nawaz, A. Malik, M. I. Choudhary, Isolation and cholinesterase-inhibition studies of sterols from haloxylon recurvum, Bioorganic & medicinal chemistry letters 16 (3) (2006) 573–580.

[13] M. Yawer, E. Ahmed, A. Malik, M. Ashraf, M. Rasool, N. Afza, New lipoxygenase-inhibiting constituents from calligonum polygonoides. chem biodiverse 4: 1578-1585 (2007).

[14] A. J. Kiessling, C. K. McClure, The conversion of amides to esters with meerwein's reagent. application to the synthesis of a carfentanil precursor., Synthetic communications 27 (5) (1997) 923–937.

Available online at www.rpnsci.com

ISSN (P): 3006-8452, ISSN (O): 3006-8460

Research Prospects in Natural Sciences, Vol. 2, Issue 1, (2024) 5–8

Research Article

Methanolic extracts of grapefruit (*Citrus paradesi*) peel, pulp and seed and their antioxidant activity

Zafar Iqbal[a,*], Amna Shaheen[b], Aisha Naz[b], Mian Habib ur Rehman Mahmood[b], Abeera Zafar[c], Muhammad Khalid Saeed[d]

[a]*Applied Chemistry Research Centre, PCSIR Labs. Complex, Lahore 54600, Pakistan*
[b]*Department of Chemistry, University of Education, Township, Lahore 54770, Pakistan*
[c]*Department of Pharmacy, Hujvery University, Lahore 54660, Pakistan*
[d]*Food & Biotechnology Research Centre, PCSIR Labs. Complex, Lahore 54600, Pakistan*

Abstract

Fresh grapefruits (*Citrus paradesi*) were collected from the vegetable market of Lahore Division, Punjab Pakistan. Their peel, pulp, and seed were subjected to drying and grinding which was followed by extraction with methanol. These methanolic extracts were further investigated to check their antioxidant activities by using 2,2-diphenyl-1-picryl-hydrazyl (DPPH). The antioxidant activities showed that the grapefruit peel methanolic extract with concentrations of 25μL, 50μL, 75μL, and 100μL has DPPH inhibition 73.6%, 76.4%, 78.8%, and 82.7% respectively. While the grapefruit pulp methanolic extract having concentrations 25μL, 50μL, 75μL, and 100μL has DPPH inhibition 60.3%, 67.3%, 73.6%, and 78.9% respectively and the grapefruit seed methanolic extract with concentrations 25μL, 50μL, 75μL, and 100μL has DPPH inhibition 59.1%, 65.7%, 71.5%, and 75.9% respectively. The results of these extracts were concentration-dependent.

Keywords:
Grapefruit, Peel, Pulp, Seed, Methanolic Extract, Antioxidant activity, DPPH.

1. Introduction

Grapefruit (*Citrus paradesi*) belongs to the Rutaceae family and it is produced by a natural cross between sweet orange (*Citrus sinensis L. Osb.*) and pummelo (*Citrus grandis L.*) [1, 2]. Its tree grows to a height of 5.6-6 m and the fruit has a diameter of approximately 15cm. The fruit is protected by a peel that demonstrates 11-14 segments, or carpels, a sheet of membrane covers each segment or carpel and each carpel contains seeds and juice sacs [3]. In 2019, world grapefruit production was 9504.1 thousand tonnes from which Asia contributed 7115.6 thousand tonnes while Pakistan and some other countries contributed 21.8 thousand tonnes [4]. In Pakistan, 95% of the total production of citrus fruits is produced by the province of Punjab from which grapefruit cultivation over five thousand hectares constitutes only 0.3% of the overall citrus production. It is predominantly grown in the subtropical regions of central Punjab, including, Sahiwal, Layyah, Sargodha, Toba Tek Singh and Khanewal. The main commercially cultivated grapefruit varieties are Foster Pink (seedy) and Shamber (seedless). Its harvesting commences in September-October, while the fruit is still green and the flesh color is not fully matured [1, 2].

Grapefruit is a rich source of nutrient, bioactive components and phytochemicals. The components include vitamin C, polyphenols, lycopene, fiber and pectin [5].These components play a significant role in providing potential health benefits because of their nutritional, antiallergic, antioxidant, anticarcinogenic and antimicrobial properties [6].

Methanolic extraction is carried out to extract bioactive components from grapefruit seed, pulp and peel to determine their antioxidant activities [7]. Antioxidants play a crucial role in safeguarding lipids and oils in food from oxidative degradation. When incorporated into food, antioxidants manage the onset of rancidity, slow down the generation of harmful oxidation byproducts, preserve nutritional quality, and prolong the shelf life of products. The natural and inherent antioxidants found in spices contribute to mitigating oxidative stress. This form of stress, resulting from elevated levels of free radicals in tissues and cells, can be triggered by diverse factors, including X-ray,

*Corresponding Author:
zafarmayo2000@yahoo.com (Zafar Iqbal)

gamma and UV radiation, contaminated food, vigorous physical activity, alcoholism, psychological stress, smoking, and adverse environmental conditions [8].

The significance of natural antioxidants lies in their ability to neutralize harmful free radicals in the body. These compounds play a crucial role in protecting cells from oxidative stress, which is linked to various chronic diseases and aging processes. Consuming a diet rich in natural antioxidants, found in fruits, vegetables, and other whole foods, can contribute to overall health by reducing the risk of oxidative damage and promoting well-being [9].

Several studies have been reported to investigate the antioxidant properties in edible parts and juice of different origin and varieties oranges [10–12]. Research has been conducted on citrus peel extracts to investigate their phytochemical and antioxidant profile [13]. The antioxidant activity of extract obtained from grapefruit seed on vegetable oils was studied [14]. The phenolic profile and antioxidant activity of some citrus fruits was also determined [15]. The purpose of this research is to obtain the methanolic extract of grapefruit seed, peel, pulp and to contribute valuable insights into the characteristics and efficiency of these extracts as antioxidant and enhance our understanding of their potential benefits.

2. Materials and Methods

2.1. Collection of Material

The fresh grapefruits were collected from the vegetable market of Lahore Division, Punjab Pakistan. Their peel, pulp and seed were separated, kept under the shade and dried for 21 days.

2.2. Chemicals

Both the reagents were of analytical grade and purchased from local market of Lahore Division, Punjab Pakistan. These include methanol and 2,2-diphenyl-1-picryl-hydrazyl (DPPH).

2.3. Methanolic Extraction

2.3.1. Grapefruit Peel

The peels of grapefruit were grounded to obtain powder by using grinder machine and passed through 500mm mesh. 100g from this powdered sample with 500ml of methanol were taken in 1000ml closed container. This mixture was allowed to macerate for 14 days with frequent shaking. After the maceration period, mixture was filtered with the help of filter paper to remove the solid residue from the liquid extract. Then, concentrated this liquid extract to evaporate the solvent by distillation method. These concentrates were then kept in air tight sample bottles and stored at room temperature.

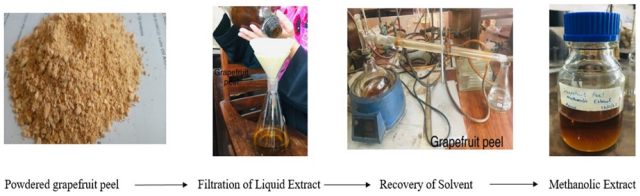

2.3.2. Grapefruit Pulp

After drying, the pulp of grapefruit was pulverized using a grinder machine to obtain powder. A 100g portion of this powdered sample combined with 500ml of methanol in a 1000ml sealed container. The mixture left to macerate for 14 days with regular shaking. Following the maceration period, the mixture was filtered using filter paper to separate the solid residue from the liquid extract. Subsequently, the liquid extract was concentrated through distillation to evaporate the solvent. The resulting concentrates were then transferred to airtight sample bottles and stored at room temperature.

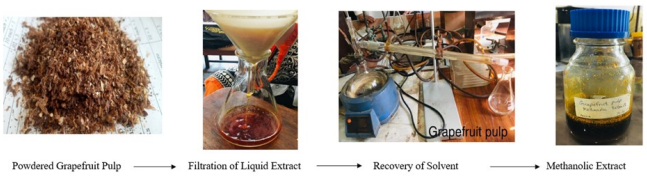

2.3.3. Grapefruit Seed

Upon completion of the drying process, dried seeds were grounded into a powder using a grinder machine to increase their surface area. After which, 100 g portion of this powdered sample along with 500 ml of methanol was taken in a sealed 1000 ml container. The mixture underwent a 14-day maceration period with frequent shaking. After maceration, the mixture was filtered using filter paper to separate the solid residue from the liquid extract. The liquid extract was subsequently concentrated through distillation to recover the solvent. The resulting concentrates were transferred to airtight sample bottles and stored at room temperature.

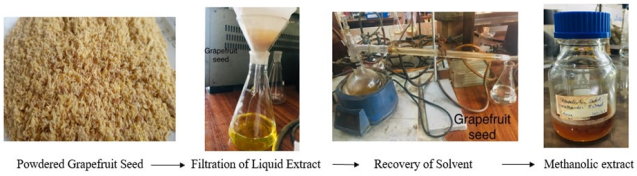

2.4. Antioxidant Activity of Methanolic Extracts

Antioxidant Activity of methanolic extracts of grapefruit were analyzed by 2,2-diphenyl-1-picryl-hydrazyl (DPPH) radical by using the method described by [16]. The extracts with various concentrations of 25μL, 50μL, 75μL and 100μL were mixed with 3 ml of methanol containing DPPH solution. The absorbance of the resulting solution and the blank (containing only DPPH) was measured at a wavelength of 517nm using a UV-Vis spectrophotometer after a 30-minute incubation at room temperature. The percentage inhibition of these extract is determined by using following equation

$$\% \text{ Inhibation (DPPH)} = \frac{Absorbance\ of\ blank\ solution - Absorbance\ of\ sample}{Absorbance\ of\ blank\ solution} \times 100$$

3. Results

3.1. Antioxidant Activity of Grapefruit Peel Methanolic Extract

The mehanolic extract of grapefruit peel showed high DPPH inhibition due to presence of high concentration of phenolic contents. These contents included a large number of volatile components e.g; limonene, ascorbic acid (vitamin C), anthocyanins, flavonoids etc. [17]. The results showed that the grapefruit peel methanolic extract with concentrations of 25μL, 50μL, 75μL and 100μL has DPPH inhibition of 73.6%, 76.4%, 78.8% and 82.7% respectively. These results have been shown in fig.(1)

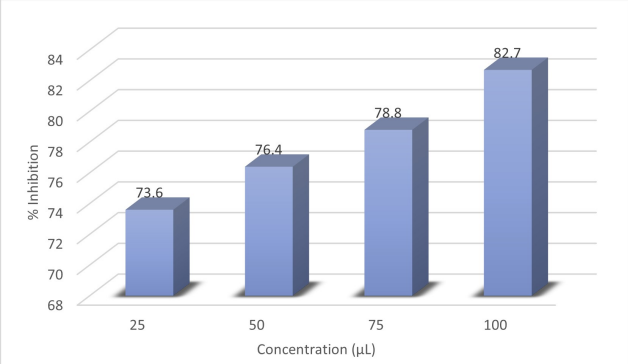

Figure 1: Antioxidant activity of Peel Methanolic Extract of Grapefruit

3.2. Antioxidant Activity of Grapefruit Pulp Methanolic Extract

The chemical composition of grapefruit pulp shows the presence of carotenoids e.g.,
beta-carotene, sugars e.g., glucose, fructose, sucrose, organic acids e.g., citric acid quininic acid and volatile components e.g., d-limonene, caryophyllene and tert-butyl 2-methylpropanoate etc [18]. The antioxidant activity of methanolic extract of grapefruit pulp is due to the presence of the voltatile components. Results showed that grapefruit pulp methanlic extract with concentrations of 25μL, 50μL, 75μL and 100μL has DPPH inhibition 60.3%, 67.3%, 73.6% and 78.9% respectively as shown in fig.(2)

3.3. Antioxidant Activity of Grapefruit Seed Methanolic Extract

The grapefruit seed contain a large number of bioactive components. These include fatty acids (linoleic acid, stearic acid, palmitic acid, and oleic acid etc), falvonoids (naringin eriocitrin, naringenin, rutin, hesperidin, and kaempherol etc), phenolic acids (gallic acid, rosmaniric acid, syringic acid and tr-2-hydrocinnamic acid etc), carotenoids (β-carotene), and volatile components (d-limonene, furfural, γ-Terpinene, and α-Terpinolene etc) [19]. The results of antioxidant activity of showed that methanolic extract of grapefruit seed with concentrations 25μL, 50μL, 75μL and 100μL has DPPH inhibition of 59.1%, 65.7%, 71.5% and 75.9% respectively, as shown in fig.(3)

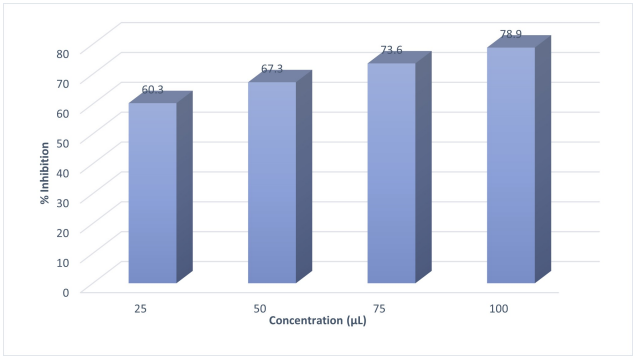

Figure 2: Antioxidant Activity of Pulp Methanolic Extract of Grapefruit

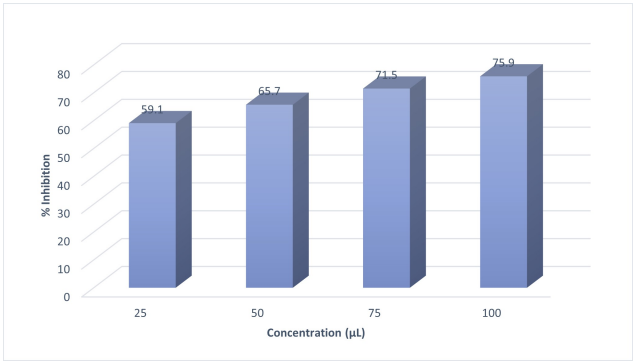

Figure 3: Antioxidant Activity of Seed Methanolic Extract of Grapefruit

4. Discussion

Literature reported that the antioxidant activity of fruits and vegetables is due to the presence of polyphenolic and phenolic compounds [20, 21]. The phenolic compounds that show antioxidant activity included ascorbic acid (vitamin C), anthocyanins, flavonoids. The antioxidant activity increases with the increase in the concentration of the phenolic and polyphenolic compounds as they were concentration-dependent. The grapefruit peel show higher antioxidant actrivity than seed and pulp [17, 22, 23]. Because peels of grapefruit and other citrus fruits have larger amounts of polyphenols as compared to peeled fruits [24]. It was also reported that the dried peel extracts of lemon, orange and mandarin show higher antioxidant acitivity due to higher concentration of phenolic contents than the fresh ones [25–28]. Citrus fruits are abundant in phenolic acids, which exhibit varying degrees of free radical scavenging. The antioxidant activity of phenolic compounds is due to the presence of phenolic hydroxyl groups that readily donate a hydrogen atom or an electron to a free radical, and an extended conjugated aromatic system that facilitates the delocalization of an unpaired electron [29]. The relationship between overall phenolic concentration and antioxidant activity has been extensively investigated across various food items, including fruits and vegetables. Prior research has shown a direct correlation between phenolic content and antioxidant capacity in fruits and

vegetables [30]. The grapefruit methanolic extract exhibited DPPH values range from 73.6% to 82.7% in peel , 60.3 to 78.9% in pulp and 59.1 to 75.9% in seeds with concentration range from 25μL to 100μL in each sample. Their antioxidant activities was represented by order as follows: peel > pulp > seed. These results are similar to Jang, Chang et al. 2010 [31], who reported that peel of pummelo had higher antioxidant activity than its pulp when employing the DPPH method. It was because methanolic extract of grapefruit peel had higher concentration of phenolic content than pulp and seed methanolic extracts of grapefruit.

References

[1] I. M. Siddique, N. Sharif, Comparative studies on pigmented grapefruit (citrus paradisi macf.) cultivars under climatic conditions of sahiwal, punjab.

[2] M. Usman, W. Rehman, B. Fatima, M. Shahid, A. H. Saggu, M. A. Rana, A. Fatima, Fruit quality assessment in pigmented grapefruit (citrus paradisi macf.) for varietal diversification, Pak. J. Agri. Sci 57 (4) (2020) 1029–1034.

[3] J. M. Cristóbal-Luna, I. Álvarez-González, E. Madrigal-Bujaidar, G. Chamorro-Cevallos, Grapefruit and its biomedical, antigenotoxic and chemopreventive properties, Food and Chemical Toxicology 112 (2018) 224–234.

[4] FAO, Citrus fruit statistical compendium 2020 (2021).

[5] W. Xi, G. Zhang, D. Jiang, Z. Zhou, Phenolic compositions and antioxidant activities of grapefruit (citrus paradisi macfadyen) varieties cultivated in china, International journal of food sciences and nutrition 66 (8) (2015) 858–866.

[6] S. Kawaii, Y. Tomono, E. Katase, K. Ogawa, M. Yano, Quantitation of flavonoid constituents in citrus fruits, Journal of Agricultural and Food Chemistry 47 (9) (1999) 3565–3571.

[7] W. Bronner, G. Beecher, Extraction and measurement of prominent flavonoids in orange and grapefruit juice concentrates, Journal of chromatography A 705 (2) (1995) 247–256.

[8] H. H. Naing, H. H. Win, N. N. Aung, A. L. Soe, Investigation of some physicochemical properties, antimicrobial activities and antioxidant activity of the citrus paradisi macfad (grapefruit).

[9] B. Halliwell, Antioxidants in human health and disease, Annual review of nutrition 16 (1) (1996) 33–50.

[10] N. J. Miller, C. A. Rice-Evans, The relative contributions of ascorbic acid and phenolic antioxidants to the total antioxidant activity of orange and apple fruit juices and blackcurrant drink, Food Chemistry 60 (3) (1997) 331–337.

[11] P. Rapisarda, A. Tomaino, R. Lo Cascio, F. Bonina, A. De Pasquale, A. Saija, Antioxidant effectiveness as influenced by phenolic content of fresh orange juices, Journal of agricultural and food chemistry 47 (11) (1999) 4718–4723.

[12] W. G. Roberts, M. H. Gordon, Determination of the total antioxidant activity of fruits and vegetables by a liposome assay, Journal of Agricultural and Food Chemistry 51 (5) (2003) 1486–1493.

[13] H. Ashraf, Iahtisham-Ul-Haq, M. S. Butt, G. A. Nayik, S. Ramniwas, T. Damto, S. Ali Alharbi, M. J. Ansari, Phytochemical and antioxidant profile of citrus peel extracts in relation to different extraction parameters, International Journal of Food Properties 27 (1) (2024) 286–299.

[14] C. Armando, S. Maythe, N. P. Beatriz, Antioxidant activity of grapefruit seed extract on vegetable oils, Journal of the Science of Food and Agriculture 77 (4) (1998) 463–467.

[15] A. Fejzić, S. Ćavar, Phenolic compounds and antioxidant activity of some citruses, Bulletin of the Chemists and Technologists of Bosnia and Herzegovina 42 (2014) 1–4.

[16] A. L. Dawidowicz, D. Wianowska, M. Olszowy, On practical problems in estimation of antioxidant activity of compounds by dpph method (problems in estimation of antioxidant activity), Food chemistry 131 (3) (2012) 1037–1043.

[17] K. A. Sir Elkhatim, R. A. Elagib, A. B. Hassan, Content of phenolic compounds and vitamin c and antioxidant activity in wasted parts of sudanese citrus fruits, Food science & nutrition 6 (5) (2018) 1214–1219.

[18] H. Zheng, Q. Zhang, J. Quan, Q. Zheng, W. Xi, Determination of sugars, organic acids, aroma components, and carotenoids in grapefruit pulps, Food chemistry 205 (2016) 112–121.

[19] E. Yilmaz, B. Aydeniz Guneser, S. Ok, Valorization of grapefruit seeds: cold press oil production, Waste and Biomass Valorization 10 (2019) 2713–2724.

[20] C. G. Fraga, M. Galleano, S. V. Verstraeten, P. I. Oteiza, Basic biochemical mechanisms behind the health benefits of polyphenols, Molecular aspects of medicine 31 (6) (2010) 435–445.

[21] S. Wang, J. P. Melnyk, R. Tsao, M. F. Marcone, How natural dietary antioxidants in fruits, vegetables and legumes promote vascular health, Food Research International 44 (1) (2011) 14–22.

[22] K. Ghasemi, Y. Ghasemi, M. A. Ebrahimzadeh, Antioxidant activity, phenol and flavonoid contents of 13 citrus species peels and tissues, Pak J Pharm Sci 22 (3) (2009) 277–281.

[23] D. Molina-Quijada, L. Medina-JuÃ¡rez, G. GonzÃ¡lez-Aguilar, R. Robles-SÃ¡nchez, N. GÃ¡mez-Meza, Phenolic compounds and antioxidant activity of table grape (vitis vinifera l.) skin from northwest mexico, CyTA-Journal of Food 8 (2010) 57–63.

[24] S. Fattouch, P. Caboni, V. Coroneo, C. I. Tuberoso, A. Angioni, S. Dessi, N. Marzouki, P. Cabras, Antimicrobial activity of tunisian quince (cydonia oblonga miller) pulp and peel polyphenolic extracts, Journal of Agricultural and Food Chemistry 55 (3) (2007) 963–969.

[25] S.-M. Jeong, S.-Y. Kim, D.-R. Kim, S.-C. Jo, K. Nam, D. Ahn, S.-C. Lee, Effect of heat treatment on the antioxidant activity of extracts from citrus peels, Journal of agricultural and food chemistry 52 (11) (2004) 3389–3393.

[26] G. Xu, X. Ye, J. Chen, D. Liu, Effect of heat treatment on the phenolic compounds and antioxidant capacity of citrus peel extract, Journal of Agricultural and Food chemistry 55 (2) (2007) 330–335.

[27] S.-C. Ho, C.-C. Lin, Investigation of heat treating conditions for enhancing the anti-inflammatory activity of citrus fruit (citrus reticulata) peels, Journal of agricultural and food chemistry 56 (17) (2008) 7976–7982.

[28] L. Castro-Vazquez, M. E. Alañón, V. Rodríguez-Robledo, M. S. Pérez-Coello, I. Hermosín-Gutierrez, M. C. Díaz-Maroto, J. Jordán, M. F. Galindo, M. d. M. Arroyo-Jimenez, et al., Bioactive flavonoids, antioxidant behaviour, and cytoprotective effects of dried grapefruit peels (citrus paradisi macf.), Oxidative Medicine and Cellular Longevity 2016.

[29] J. Dai, R. J. Mumper, Plant phenolics: Extraction, analysis and their antioxidant and anticancer properties, Molecules 15 (10) (2010) 7313–7352.

[30] B. Li, B. Smith, M. M. Hossain, Extraction of phenolics from citrus peels: I. solvent extraction method, Separation and Purification Technology 48 (2) (2006) 182–188.

[31] H.-D. Jang, K.-S. Chang, T.-C. Chang, C.-L. Hsu, Antioxidant potentials of buntan pumelo (citrus grandis osbeck) and its ethanolic and acetified fermentation products, Food chemistry 118 (3) (2010) 554–558.

Available online at www.rpnsci.com

ISSN (P): 3006-8452, ISSN (O): 3006-8460

Research Prospects in Natural Sciences Vol. 2, Issue 1, (2024) 9–11

Research Article

Evaluation and extraction of natural hair colors from different herbal and dry fruit items for formulation

Lubna Liaquat[a], Phool Shahzadi[a,*], Azra Yaqoob[a], Zeeshan Ali[a], Zahida Parveen[a], Alim-un-Nisa[a], Usman Saeed Kiani[b], Razia Kalsoom[c]

[a]*PCSIR Laboratories Complex, Lahore 54600, Pakistan*
[b]*Institute of metallurgy and materials engineering, Univeristy of the Punjab, Lahore 54000, Pakistan*
[c]*PCSIR Laboratories Complex, Islamabad, Pakistan.*

Abstract

In the present investigation, attempts were made to make a powder herbal hair dye resembling natural hair color with better dyeing effect, superior quality, long-lasting, and hundred percent pure. Synthetic hair dye includes dye modifiers, antioxidant alkalizers, soap ammonia, wetting agents, fragrances, and a variety of other softening agents that are harmful to health and cause cancer. To overcome these problems in the present investigation, we developed a method to get a natural brown color using a combination of different plant materials, i.e., amla (*Emblica officinalis gaertin*), olive (*Olea europaea*), almond peel, and peanut peels. The current study examined several combinations of hair-care plants, including henna, peanut, almond, walnut, indigo, and aloe vera. Additionally, basic and inexpensive ingredients were used, saving money and foreign exchange. We get brown hair naturally from these raw materials, which are themselves medicines for hair growth and have an endless list of therapeutic benefits that antimicrobial antiseptic, and anti-inflammatory herbs impart. Brown color and a scalp free from dandruff ensure quality with no side effects. It is pharmacologic invention for ageing hair, which is a vital alteration for synthetic hair dye. It is a 100% natural source. A natural herbal hair dye is an excellent colorant for all types of hair because synthetic dyes have the chief disadvantage of causing preventive reactions and hair loss. All natural hair dyes are made from plants using the latest scientific achievements in green chemistry. The result obtained from the brown hair dye process investigation confirmed that hair dye prepared from hulls was excellent and economical, with a number of benefits for hair.

Keywords:
Henna, Peanut Hull, Natural herbs, Almond Hull, Black Tea, Aloe vera.

1. Introduction

Continuously using permanent or semi-permanent hair color dye along with hair dye shampoo can heighten the likelihood of long-term exposure to synthetic hair dye chemicals, thus potentially elevating the risk of breast cancer development [1]. Hair dye A need was felt to formulate the product containing only plant products and develop a hair dye alternative to synthetic dyes / having metals salt base. The natural brown hair dye from natural sources and natural ingredients which is safe for use of hyper sensitive reaction [2]. Brown hair dyes derived from henna provide a natural hue to the hair, distributing evenly across the scalp, and resulting in fragrant, soft, and easily manageable hair. Hair dyes derived from natural sources address issues [3] like hair cuticle damage, irritation, and scalp sensitivity. They are safe to use and don't pose problems such as skin staining, itching, or hypersensitive reactions. Products using plant-based colorants, sourced from various renewable sources, are generally considered environmentally friendly and bio-compatible [4]. The natural brown hair dye possesses full penetration to be used as coloring agent and safe hair colorant [5]. Hair dye is important cosmetic item for not only men but also for women. Now a days, oxidation dyes account for around 80% of the hair colorant industry, with the remaining non-oxidative segment which is based on synthetic organic dyes representing the remaining market, with the exception of a very small portion that is made up of lead acetate and natural colors [6]. Synthetic dye-based or permanent hair dyes typically consist of two components: color and developer. The color component typically includes various synthetic dyes and intermediates such as ammonia, diaminobenzene, phenyldiamine, resorcinol,

*Corresponding Author:
psk717@gmail.com (Phool Shahzadi)

Table 1. Ingredients Formulation for Medium Brown

Name of Hair Dye	Shade	Ingredients	Composition
H1 (Hair dye)	Medium Brown	Henna	30-35 %
		Indigo	3-7 %
		Aloe vera	5-7 %
		Peanut Hull	8-10 %
		Walnut Hull	8-12 %
		Gram Hull	8-10 %
		Pine nut Hull	8-10 %
		Almond Hull	8-12 %
		Black gram	2-3 %
		Laung	3-5 %
		Alum	2-3 %
		Lemon	3-5 %
		Black Tea	2-5 %

Table 2. Ingredients Formulation for Pale Yellow

Name of Hair Dye	Shade	Ingredients	Composition
H2 (Hair dye)	Pale Yellow	Henna	35-40 %
		Indigo	5-7 %
		Aloe vera	5-7 %
		Peanut Hull	7-10 %
		Walnut Hull	7-10 %
		Gram Hull	3-4 %
		Pine nut Hull	6-9 %
		Almond Hull	7-9 %
		Black gram	2-3 %
		Laung	3-5 %
		Alum	2-3 %
		Lemon	3-5 %

ortho-para-aminophenol, p-toluenodiamine, green ingredients, and their variants. These ingredients, often in forms like HCl or sulfate (e.g., PPP), are potent irritants and have been linked to allergic reactions [7]. Other irritant ingredients include H_2O_2 naphthol. The release of reactive oxygen species (ROS) following dye exposure is another factor that may lead to skin allergies [8, 9]. Hair dye sold in the European Union containing any of the listed ingredients must carry a warning due to their potential to cause allergic reactions and penetrate the skin, leading to a risk of cancer. Prolonged use of such hair dye typically results in local irritation and skin toxicity. It can also manifest as blisters, itching, rashes, pigmentation issues, and in some cases, serious dermatological disorders, indicating a wide range of potential biological effects [2, 10]. In spite of above disadvantage natural dye possess some limitation and technical draw back like color yield, higher cost, limited shades, low fastness properties and blending problems. The increase in synthetic dyes over the past three centuries has led to the neglect of natural dyes, resulting in a decrease in research efforts dedicated to them [5, 11]. To address the limitations of natural dyes, a systematic scientific approach can be employed. The active constituents also offer protection against hair damage caused by photo reactions and pollution. This formulation has been demonstrated to be a viable alternative to synthetic and semi-synthetic dyes in vitro. In the current study, a formulation has been developed to achieve a natural brown color using a combination of natural ingredients. The primary objective of this investigation is to formulate a hair color that is both natural and safe.

2. Materials and Methods

2.1. Production Profile

The present investigation provides a process for the preparation of herbal hair dye. The plants used in the study are Henna (*Lawsonia viernis Lim*), Indigo, Aloe vera, *Sapindu mucrorosia*, *Embica officinalis*, olive, Walnut Hull, Peanut Hull, Almond Hull were collected, dried in shade till they contain moisture less than 2-3%by mass.

The shade dried weighed plant were crushed to powder form by using electrical speeder. The powdered form material has tannin or coloring agent [12]. The fine powder raw material was soaked in water

1. Weighed quantity of Henna (*Lawsonia viernis Lim*) mix with sugar.
2. Grinding the Indigo, Aloe vera, and olive homogenously.
3. Grinding the Peanut Hull, Almond Hull and Black Walnut Hull.
4. Soaking above ingredients into the bowl.
5. Boil at simmering point 85-90°C for time period of 30-50 min.
6. Filter it after boiling.
7. The filtrate added in mixture of Henna, Sugar, Vinegar Laung and small quantity of alum under constant vigorous stirring at moderate temperature maintained ph 7-8.
8. Dry it at room temperature
9. The powder from colored hair dye was formulated with suitable ratio of low or high quantity under safe limits to obtain the required composition. It is like a part adding a fragrance agent applied to the hair for light or dark brown shade.

Table 3. Ingredients Formulation for Dark Brown

Name of Hair Dye	Shade	Ingredients	Composition
H3 (Hair dye)	Dark Brown	Henna	25-30 %
		Indigo	2-5 %
		Aloe vera	3-5 %
		Peanut Hull	5-8 %
		Walnut Hull	10-12 %
		Gram Hull	10-12 %
		Pine nut Hull	10-12 %
		Almond Hull	10-12 %
		Black gram	2-3 %
		Laung	5-5 %
		Alum	2-3 %
		Lemon	3-5 %
		Black Tea	3-7 %

2.2. Brown Herbal Hair Dye Preparation

The henna Black tea, sugar lemon, Almond peel, Peanut Pel Walnut Hull etc were collected from different places and dried

Table 4. Herbal Hair Dye

S. No.	Name of Hair Dye	Herbal Hair Dye	Coloring effect or fastness properties	Duration of retaining/permence	Physical Appearance
1	H1 (Hair dye)	Medium Brown (H1)	4/5 to 5	2-3 months	Very good to excellent
2	H2 (Hair dye)	Pale Brown (H2)	4/5 to 5	2-3 months	Very good to excellent
3	H3 (Hair dye)	Dark Brown (H3)	4/5 to 5	2-3 months	Very good to excellent

in shade for maintain it color an ph. After processing they were crushed into powder and used for the preparation of brown hair colorant [13].

2.3. Collection of unpigmented hair

The human white hair was collected from the barber shops and also from our aged colleague. Suitable combination of different ingredients with henna, 10g aloe vera, 5g indigo, 5g olive, 2g walnut hull, 2g peanut hull, 1g almond skin hull, after crushing into powder for mixed well and (2g black tea and 10 ml water) was added to water in order to make smooth paste. The paste was kept aside or 1-2 hours. The white human hair was kept or put in above. Paste for 1-2 hours. Mixed well with spatula. 2-5 gm sugar and lemon juice as color preservation also added. After that it was washed with tape water and observed for its coloring. Suitable permanent color fast combination of henna and ingredients: Different ratios of henna and ingredients are mixed together to get color fast paste for human white hair and effect of pH was studied. To the paste of above ratio dilute solution of sugar and lemon juice were added in order to obtain the pH of 6,7,8, and 9.

3. Results and Discussion

Progressive natural brown hair dyes offer superior dyeing effects with increased retention capacity, resulting in long-lasting color. The brown shade is unique with its natural characteristics, and immediate results can often be achieved with just one application. One of the key advantages of this brown hair color is its ability to avoid irritation, itching, dandruff, and scalp weakness, while simultaneously providing hair with strength and luster [14].

Natural hair dyes like black walnut powder, almond, peanut hull, indigo, aloe vera, olive, sugar, black tea, lemon, etc., are potent and effective options for dyeing hair naturally. These ingredients are also beneficial for eliminating dandruff and promoting hair growth. In the preparation of brown herbal hair dye, ingredients such as henna, black tea, sugar, lemon, almond peel, and walnut peel are utilized, offering a safe option without side effects [15]. Conversely, chemical-oriented products may provide quick results but can also lead to serious side effects. To address these concerns, opting for herbal hair dyes with attractive shades is recommended.

4. Conclusion

Hair color dyeing is only one of the technologies involved in getting the right color on to the right herbal dye materiel in order to use it effectively. The hair dyeing will need at least one day addition and probably several to achieve the correct or fast hair dye.

References

[1] M. Huncharek, B. Kupelnick, Personal use of hair dyes and the risk of bladder cancer: results of a meta-analysis, Public health reports 120 (1) (2005) 31–38.
[2] S. P. Phadatare, T. N. Nesari, D. Pokharkar, R. Pingle, M. Gadge, Comparative study of dyeing efficiency and retention capacity of herbal hair dyes., International Journal of Research in Ayurveda & Pharmacy 4 (2).
[3] G. H. Rauscher, D. Shore, D. P. Sandler, Hair dye use and risk of adult acute leukemia, American journal of epidemiology 160 (1) (2004) 19–25.
[4] H. Cui, R. Cai, Z. Hua, Y. Tang, Plant colorants for natural hair coloration: Dyeing optimization and photostability assessment, Sustainable Chemistry and Pharmacy 36 (2023) 101285.
[5] T. Bechtold, R. Mussak, Handbook of natural colorants, Vol. 8, John Wiley & Sons, 2009.
[6] J. F. CORBETT, 10 synthetic dyes for human hair, Colorants for non-textile applications (2000) 456.
[7] V. Kapoor, Herbal cosmetics for skin and hair care.
[8] T. B. Zanoni, T. N. Pedrosa, C. M. Catarino, S. W. Spiekstra, D. P. de Oliveira, G. Den Hartog, A. Bast, G. Hagemann, S. Gibbs, S. B. de Moraes Barros, et al., Allergens of permanent hair dyes induces epidermal damage, skin barrier loss and il-1 α increase in epidermal in vitro model, Food and chemical toxicology 112 (2018) 265–272.
[9] S. Wang, J. Chen, Z. Jin, Y. Xing, R. Wang, Natural hair color and skin cancers: A two-sample mendelian randomization study, Gene 893 (2024) 147940.
[10] P. Pahade, A. Durgbanshi, S. Carda-Broch, J. Peris-Vicente, D. Bose, Micellar enhanced chromatographic separation of selected hazardous chemical present in hair dye and their detection in formulations and swab, including assessment of damage caused to cuticle of hair shaft, Journal of Chromatography A 1705 (2023) 464206.
[11] Y. M. Rao, P. Sujatha, et al., Formulation and evaluation of commonly used natural hair colorants, Natural Product Radiance 7 (1) (2006) 45–48.
[12] The world of hair color, 62-89, Thomson harming Landon, 2005.
[13] N. Packianathan, S. Karumbayaram, Formulation and evaluation of herbal hair dye: an ecofriendly process, Journal of Pharmaceutical Sciences and Research 2 (10) (2010) 648.
[14] S. D. Swati Deshmukh, B. K. Bindurani Kaushal, S. G. Shweta Ghode, Formulations and evaluation of herbal shampoo and comparative studies with herbal marketed shampoo.
[15] J. W. Claude Bouillon (Ed.), The science of hair care (second edition), 252-253, CRC Press, 2005.

Available online at www.rpnsci.com

ISSN (P): 3006-8452, ISSN (O): 3006-8460

Research Prospects in Natural Sciences Vol. 2, Issue 1, (2024) 13–17

Research Article

Electromagnetic wave propagation in a rectangular waveguide filled with a double-negative (DNG) metamaterial

Burhan Zamir[a,*], Zeeshan Naseer[b], Babar Shahzad[b]

[a]*Department of Physics, Govt. M. A. O. Graduate College, Lahore 54000, Pakistan*
[b]*Department of Physics, Division of Science & Technology, University of Education, Lahore 54700, Pakistan.*

Abstract

This article presents an analysis of electromagnetic wave propagation in a model of rectangular waveguide when filled with a double-negative metamaterial. The field components and dispersion relation of the electromagnetic waves are calculated, analytically. The dispersion relation is numerically analysed by plotting the normalized squared phase velocity against the propagation frequency for the variation of parameters of waveguide and the wave. The dominant mode is found to be TE^{10} mode. The dispersion curves show propagation and non-propagation characteristics for larger dimensions and for dominant mode. Some aspects were found to be much different from a conventional rectangular wave-guide.

Keywords:
Rectangular waveguide, double-negative metamaterial, wave propagation.

1. Introduction

Rectangular waveguide loaded with various modern media has been the topic of current interest for the microwave communication device applications such as filters, isolators, couplers, sensors etc. [1–4]. In modern microwave materials, the double-negative (DNG) metamaterials show very interesting properties as compared to the conventional double-positive (DPS) dielectrics. Vesselago [5] suggested the plane wave propagation in a medium containing simultaneously negative permittivity and permeability. This idea then experimentally realized by Pendry et al. [6–8], Smith et al. [9], and Shelby et al. [10]. Now, the DNG materials have been studied in different waveguides and cavities for different applications such as low-pass, high-pass and multiband filters etc. [11–15]. These applications have been revealed by various authors. For example, Weng et al. [1] used accurate rigorous modal theory to study rectangular waveguide filled with multilayer right and left handed metamaterials and shown the multiband propagation properties below cut-off. Moradi [2] studied a rectangular waveguide filled with anisotropic medium by using electrostatic theory of the wave propagation and proposed its applications in microwave regime. In another work, Weng et al. [3] investigated the rectangular waveguide filled with graded inhomogeneous metamaterial for the wave propagation and suggested a new approach for the waveguide miniaturization.

In above discussed waveguides, the medium filled in the waveguide played the key role for their applications. Therefore, in the current proposed study, we analyse a rectangular waveguide filled with a linear, homogeneous and isotropic double-negative (DNG) metamaterial for the possible propagation properties and applications. This article is organized as follows: section (1) represents the introduction to the current study; section (2) includes the theoretical analysis of the proposed waveguide based on electromagnetic wave theory; section (3) aims to present the numerical results with discussion, and section (4) focuses on the conclusion.

2. Theoretical analysis

Consider a rectangular waveguide with perfect electrical conducting (PEC) walls as shown in figure (1). The planar symmetry of the waveguide is extended in xz-plane with dimensions $y = a$ and $x = b$, whereas, the waveguide is extended infinitely along z-direction. An electromagnetic wave is considered to propagate in the z-direction with the plane wave solution profile $e^{i(\omega t - kz)}$. The medium inside the boundary walls of the waveguide is a linear, homogeneous and isotropic double-negative (DNG) material.

*Corresponding Author:
burhanzamir1@gmail.com (Burhan Zamir)

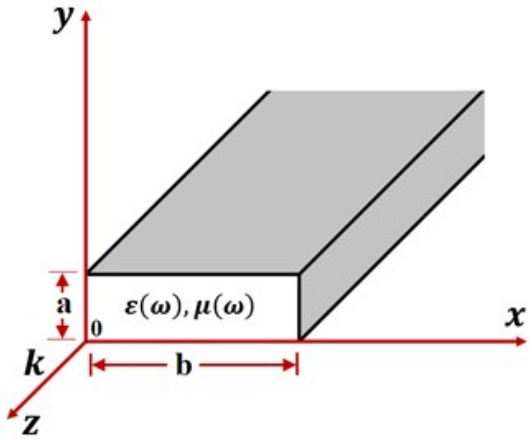

Figure 1: Model of a rectangular waveguide filled with DNG metamaterial.

A left-handed or DNG material is so-called frequency dependant material, characterized by the following expressions of relative permittivity and relative permeability [11–14].

$$\varepsilon_{_D}(\omega) = 1 - \frac{\omega_p^2}{\omega^2} \tag{1}$$

$$\mu_{_D}(\omega) = 1 - \frac{F\omega^2}{\omega^2 - \omega_r^2} \tag{2}$$

where ω is the frequency of propagation, ω_p is the plasma frequency of long metallic wires (LMW), ω_r is the resonance frequency of the split ring resonators (SRRs) and F is the filling fraction of DNG material structure. Maxwell equations for the DNG material can be written as

$$\nabla \times H = i\omega\varepsilon_{\circ}\varepsilon_{_D}(\omega)E \tag{3}$$

$$\nabla \times E = -i\omega\mu_{\circ}\mu_{_D}(\omega)H \tag{4}$$

Coupling the above Maxwell equations, we get the following wave equations for E and H

$$\frac{\partial^2 E}{\partial x^2} + \frac{\partial^2 E}{\partial y^2} = k_D^2 E \tag{5}$$

$$\frac{\partial^2 H}{\partial x^2} + \frac{\partial^2 H}{\partial y^2} = k_D^2 H \tag{6}$$

Where $k^2 - \omega\varepsilon_D(\omega)\mu_D(\omega) = k_D^2$ Writing equations (3) and (4) in component form, the following sets of equations are obtained

$$\begin{cases} \dfrac{\partial H_z}{\partial y} + ikH_y = i\omega\varepsilon_D(\omega)E_x & (7) \\ -\dfrac{\partial H_z}{\partial x} - ikH_x = i\omega\varepsilon_D(\omega)E_y & (8) \\ \dfrac{\partial H_y}{\partial x} - \dfrac{\partial H_x}{\partial y} = i\omega\varepsilon_D(\omega)E_z & (9) \end{cases}$$

$$\begin{cases} \dfrac{\partial E_z}{\partial y} + ikE_y = -i\omega\mu_D(\omega)H_x & (10) \\ -\dfrac{\partial E_z}{\partial x} - ikE_x = -i\omega\mu_D(\omega)H_y & (11) \\ \dfrac{\partial E_y}{\partial x} - \dfrac{\partial E_x}{\partial y} = -i\omega\mu_D(\omega)H_z & (12) \end{cases}$$

Solving the above set of equations for the field components H_x, E_x, H_y, E_y in terms of H_z and E_z, we get the following expressions

$$H_x = \frac{i}{k_D^2}\left(k\frac{\partial H_z}{\partial x} + \omega\varepsilon_D(\omega)\frac{\partial E_z}{\partial y}\right) \tag{13}$$

$$E_x = \frac{i}{k_D^2}\left(\omega\mu_D(\omega)\frac{\partial H_z}{\partial y} + k\frac{\partial E_z}{\partial x}\right) \tag{14}$$

$$H_y = \frac{i}{k_D^2}\left(k\frac{\partial H_z}{\partial y} + \omega\varepsilon_D(\omega)\frac{\partial E_z}{\partial x}\right) \tag{15}$$

$$E_y = \frac{i}{k_D^2}\left(\omega\mu_D(\omega)\frac{\partial H_z}{\partial x} - k\frac{\partial E_z}{\partial y}\right) \tag{16}$$

The solution of equation (5) is obtained for E_z by using separation of variables method, given by

$$E_z = (c_1 \cos Ax + c_2 \sin Ax)\,(c_3 \cos By + ic_4 \sin By) \tag{17}$$

where $A^2 = -k_D^2 - B^2 and c_1, c_2, c_3$and c_4 are constants which can be evaluated by using appropriate boundary conditions. Now, using the boundary conditions, (i.e. the vanishing of the tangential field component at the surface of a PEC), in equation (17), we get the following solution

$$E_z = E_o \sin\left(\frac{n\pi x}{b}\right)\sin\left(\frac{m\pi y}{a}\right) \tag{18}$$

where $n = 0, 1, 2, \ldots$ and $m = 0, 1, 2 \ldots, A = n\pi/b$, $B = m\pi/a$ and $E_\circ$ is the amplitude of E_z.

2.1. TM modes

There is no magnetic field component in the direction of propagation of wave for a transverse magnetic (TM) mode, therefore, setting $H_z = 0$ in equations (13)-(16), we get the following field vectors for the TM wave modes

$$H_x = \frac{i\omega}{k_D^2}\varepsilon_D(\omega)\frac{\partial E_z}{\partial y} \tag{19}$$

$$E_x = \frac{ik}{k_D^2}\frac{\partial E_z}{\partial x} \tag{20}$$

$$H_y = \frac{i\omega}{k_D^2}\varepsilon_D(\omega)\frac{\partial E_z}{\partial x} \tag{21}$$

$$E_y = -\frac{ik}{k_D^2}\frac{\partial E_z}{\partial y} \tag{22}$$

Using the solution (18) in above equations, we get the following field components for the TM wave modes

$$H_y = \frac{i\omega\varepsilon_D(\omega)}{k_D^2}\frac{n\pi}{b}\left\{E_o\cos\left(\frac{n\pi x}{b}\right)\sin\left(\frac{m\pi y}{a}\right)\right\} \tag{23}$$

$$E_y = \frac{ik}{k_D^2}\frac{m\pi}{a}\left\{E_o\sin\left(\frac{n\pi x}{b}\right)\cos\left(\frac{m\pi y}{a}\right)\right\} \tag{24}$$

$$E_x = \frac{ik}{k_D^2}\frac{n\pi}{b}\left\{E_o\cos\left(\frac{n\pi x}{b}\right)\sin\left(\frac{m\pi y}{a}\right)\right\} \tag{25}$$

$$H_x = \frac{-i\omega\varepsilon_D(\omega)}{k_D^2}\frac{m\pi}{a}\left\{E_o\sin\left(\frac{n\pi x}{b}\right)\cos\left(\frac{m\pi y}{a}\right)\right\} \tag{26}$$

To find the expression of the dispersion relation for the TM modes, we use $A = n\pi/b$, $B = m\pi/a$ in $A^2 = -k_D^2 - B^2$ as mentioned in equations (17) and (18), we get

$$k^2 = \frac{\omega^2}{c^2}\varepsilon_D(\omega)\mu_D(\omega) - \left(\frac{n\pi}{b}\right)^2 - \left(\frac{m\pi}{a}\right)^2 \tag{27}$$

2.2. TE Modes

For the transverse electric (TE) Modes, there is no electric field component in the direction of propagation of wave. Therefore, we use $E_z = 0$ in equations (13)-(16), we get the following field vectors for the TE wave modes

$$H_x = \frac{ik}{k_D^2}\frac{\partial H_z}{\partial x} \tag{28}$$

$$E_x = \frac{i\omega}{k_D^2}\mu_D(\omega)\frac{\partial H_z}{\partial y} \tag{29}$$

$$H_y = \frac{ik}{k_D^2}\frac{\partial H_z}{\partial y} \tag{30}$$

$$E_y = \frac{i\omega}{k_D^2}\mu_D(\omega)\frac{\partial H_z}{\partial x} \tag{31}$$

For the TE modes, we solved equation (6) for H_z by using separation of variables method and use the same mathematical procedure as described in section (2.1) to find the following solution

$$H_z = H_o\cos\left(\frac{n\pi x}{b}\right)\cos\left(\frac{m\pi y}{a}\right) \tag{32}$$

where $H_\circ$ is the amplitude of H_z. The corresponding field components for the TE modes are given by

$$E_x = -\frac{i\omega\mu}{k_D^2}\left(\frac{m\pi}{a}\right)\left\{H_o\sin\left(\frac{n\pi x}{b}\right)\sin\left(\frac{m\pi y}{a}\right)\right\} \tag{33}$$

$$E_y = -\frac{i\omega\mu}{k_D^2}\left(\frac{m\pi}{a}\right)\left\{H_o\cos\left(\frac{n\pi y}{a}\right)\sin\left(\frac{m\pi x}{b}\right)\right\} \tag{34}$$

$$H_x = -\frac{ik}{k_D^2}\left(\frac{m\pi x}{b}\right)\left\{H_o\cos\left(\frac{n\pi y}{a}\right)\sin\left(\frac{m\pi x}{b}\right)\right\} \tag{35}$$

$$H_y = -\frac{ik}{k_D^2}\left(\frac{n\pi}{a}\right)\left\{H_o\sin\left(\frac{n\pi y}{a}\right)\sin\left(\frac{m\pi x}{b}\right)\right\} \tag{36}$$

In this case, the dispersion relation is the same as that of the TM wave mode, given by

$$k^2 = \frac{\omega^2}{c^2}\varepsilon_D(\omega)\mu_D(\omega) - \left(\frac{n\pi}{b}\right)^2 - \left(\frac{m\pi}{a}\right)^2 \tag{37}$$

3. Results and discussion

To analyse the proposed rectangular waveguide for the wave propagation characteristics, the dispersion relation given in equation (37) is mathematically manipulated for the normalized squared phase velocity, given by

$$\frac{v_\varphi^2}{c^2} = \left\{\varepsilon_D(\omega)\mu_D(\omega) - \left(\frac{cn\pi}{\omega b}\right)^2 - \left(\frac{cm\pi}{\omega a}\right)^2\right\}^{-1} \tag{38}$$

To investigate the dispersion characteristics of the electromagnetic wave, it is more convenient to plot normalized squared phase velocity against frequency, instead of usual wave vector-frequency plot [11]. First, we find the frequency range for which both permittivity and permeability of the DNG metamaterial have simultaneously negative values. For this purpose, a graph of equations (1) and (2) are plotted for the permittivity and permeability against the frequency, as shown in figure (2), for the parameters $F = 0.56, \omega_r = 4\times10^9 Hz and \omega_p = 10\times10^9 Hz$ [11–15]. The frequency range is found to be $4\times10^9 Hz$ and $6\times10^9 Hz$ which is in microwave frequency range.

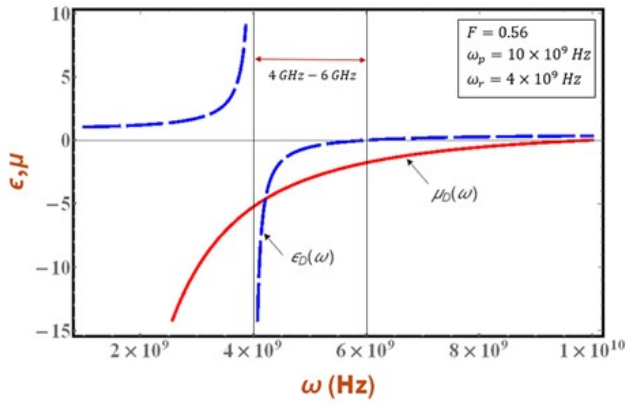

Figure 2: A graph between relative permittivity/permeability and frequency to find the existence range of a DNG material.

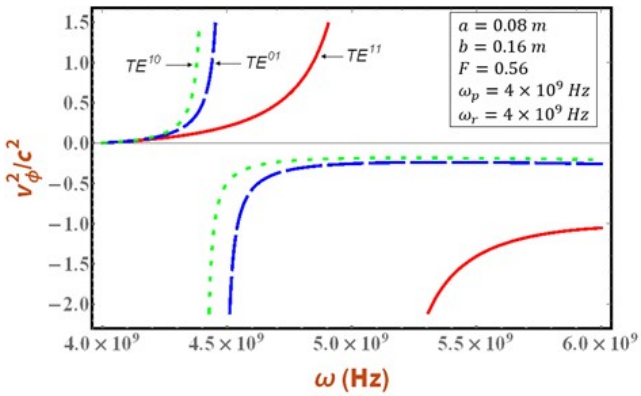

Figure 3: A plot of $\frac{v_\varphi^2}{c^2}$ versus ω for various waveguide modes and for the rectangular waveguide filled with DNG material

The dispersion characteristics are obtained by plotting equation (38) for $\frac{v_\varphi^2}{c^2}$ versus ω within the existence range of the DNG

metamaterial, as shown in figure (3). This figure shows the dispersion curves for various TE^{mn} modes i.e. TE^{10}, TE^{01}, and TE^{11} modes. Each curve shows two branches separated by a cut-off. The branch of each curve with $\frac{v_\varphi^2}{c^2} > 0$ shows the propagation of electromagnetic waves through waveguide, whereas the branch of each curve with $\frac{v_\varphi^2}{c^2} < 0$ represents non-propagation region. The frequency separating the propagation and non-propagation regions is the cut-off frequency, given by

$$\omega_c = \left[\frac{1}{\varepsilon_D(\omega)\mu_D(\omega)}\left\{\left(\frac{n\pi}{b}\right)^2 + \left(\frac{m\pi}{a}\right)^2\right\}\right]^{1/2} \tag{39}$$

Within $4GHz - 6GHz$, the wave propagation is observed for $\omega < \omega_c$, therefore, the waveguide is behaving like a low-pass filter which is different from a conventional rectangular waveguide (a waveguide filled with a usual right-handed dielectric material) for which there is no propagation found in the frequency range under consideration (see figure (4)). This property of the proposed structure may be useful as filter, sensor etc., within the microwave frequency band. It is clear from the graph that the cut-off for various wave modes are different and TE^{10} is the dominant mode.

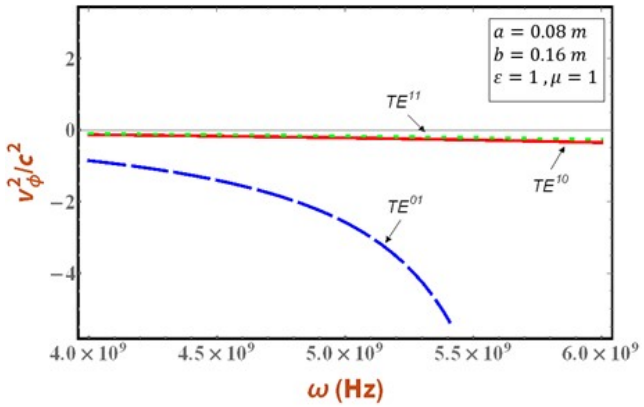

Figure 4: A plot of $\frac{v_\varphi^2}{c^2}$ versus ω for various waveguide modes and for the rectangular waveguide filled with DPS material.

To discuss the effect of the dimensions of waveguide on propagation characteristics, the dispersion relation (38) is again plotted for $\frac{v_\varphi^2}{c^2}$ versus ω for different values of the dimensions a and b and for dominant mode TE^{10}, as shown in figure (5). The dispersion curves show the same behaviour as discussed in figure (3). It is seen that by increasing the dimensions of the waveguide, the cut-off shifts to a higher frequency value and the propagation region of frequency also increases. It can further be concluded that the cut-off is a function of both, dominant mode and the waveguide dimensions. Such properties of a waveguide are useful as filters, sensor and maybe helpful in the development of microwave radars and antennas technology.

4. Conclusion

In this work, a rectangular waveguide loaded with a double-negative (DNG) metamaterial is proposed to study the propagation characteristics of the electromagnetic waves. In this connection, the dominant mode is found to be TE^{10} but the wave propagation characteristics are much different from a conventional waveguide filled with right handed dielectric. Within the existence range of a DNG material, the waveguide behaves as a low pass filter with a cut-off that increases by increasing the dimensions of the waveguide. Whereas, conventional waveguide does not show any propagation for the choice of same dimensions and the frequency band. Thus, for a particular choice of dimensions, the proposed waveguide maybe used in microwave applications such as filters, sensors, and isolators etc. within a frequency range where the conventional waveguide, loaded with right handed material, does not show any propagation.

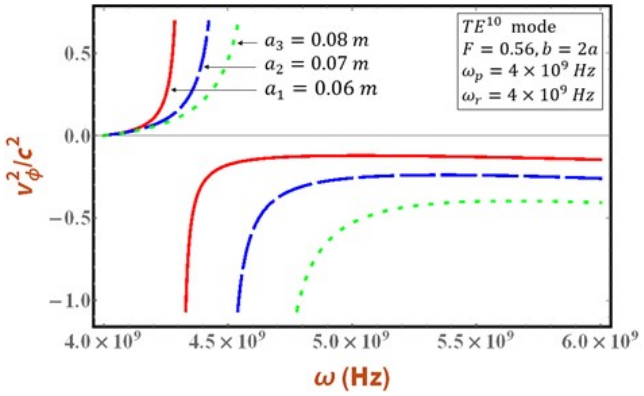

Figure 5: A plot of $\frac{v_\varphi^2}{c^2}$ versus ω for various waveguide dimensions and for the dominant mode TE^{10} of the rectangular waveguide filled with DNG material

References

[1] Q. Weng, Q. Lin, H.-F. Wu, Multiband below-cutoff propagation in rectangular waveguides filled with multilayer left-/right-handed metamaterials, Progress In Electromagnetics Research M 99 (2021) 115–127.

[2] A. Moradi, Electrostatic theory of rectangular waveguides filled with anisotropic media, Scientific Reports 11 (1) (2021) 24522.

[3] Q. Weng, Q. Lin, H. Wu, The propagation characteristics of rectangular waveguides filled with inhomogeneous double-negative dielectrics using a semianalytical method, International Journal of Numerical Modelling: Electronic Networks, Devices and Fields 34 (4) (2021) e2860.

[4] A. Refaie Ali, N. Eldabe, A. A. El Naby, M. Ibrahim, O. Abo-Seida, Em wave propagation within plasma-filled rectangular waveguide using fractional space and lfd, The European Physical Journal Special Topics 232 (14) (2023) 2531–2537.

[5] G. V. Viktor, et al., The electrodynamics of substances with simultaneously negative values of ε and μ, Soviet Physics Uspekhi 10 (4) (1968) 509.

[6] J. B. Pendry, A. Holden, W. Stewart, I. Youngs, Extremely low frequency plasmons in metallic mesostructures, Physical review letters 76 (25) (1996) 4773.

[7] J. B. Pendry, A. Holden, D. Robbins, W. Stewart, Low frequency plasmons in thin-wire structures, Journal of Physics: Condensed Matter 10 (22) (1998) 4785.

[8] J. B. Pendry, A. J. Holden, D. J. Robbins, W. Stewart, Magnetism from conductors and enhanced nonlinear phenomena, IEEE transactions on microwave theory and techniques 47 (11) (1999) 2075–2084.

[9] D. R. Smith, W. J. Padilla, D. Vier, S. C. Nemat-Nasser, S. Schultz, Composite medium with simultaneously negative permeability and permittivity, Physical review letters 84 (18) (2000) 4184.

[10] R. A. Shelby, D. R. Smith, S. Schultz, Experimental verification of a negative index of refraction, science 292 (5514) (2001) 77–79.

[11] B. Zamir, R. Ali, Wave propagation in parallel-plate waveguides filled with nonlinear left-handed material, Chinese Physics B 20 (1) (2011) 014102.

[12] I. V. Shadrivov, A. A. Sukhorukov, Y. S. Kivshar, A. A. Zharov, A. D. Boardman, P. Egan, Nonlinear surface waves in left-handed materials, Physical Review E 69 (1) (2004) 016617.

[13] B. Zamir, S. Ilyas, B. Shahzad, Te and tm surface waves at the interface of a left-handed metamaterial, Research Prospects in Natural Sciences (RPNS) 1 (1) (2023) 11–15.

[14] B. Zamir, A. Nisar, B. Shahzad, Electromagnetic wave propagation in a parallel-plate waveguide filled with linear metamaterials, Research Prospects in Natural Sciences (RPNS) 1 (1) (2023) 23–29.

[15] K. Y. Kim, Comparative analysis of guided modal properties of double-positive and double-negative metamaterial slab waveguides., Radioengineering 18 (2).

Available online at www.rpnsci.com

ISSN (P): 3006-8452, ISSN (O): 3006-8460

Research Prospects in Natural Sciences Vol. 2, Issue 1, (2024) 19–21

Research Article

Island size distribution study for rubrene thin films on muscovite mica and SiO_2 using scaling theory

Kamila Rehman[a,b], Aaliya Rehman[a,*], Shaimaa M. Abdalbaqi[b], Helmut Sitter[b]

[a]*Department of Physics, Govt. M.A.O. Graduate College, Lahore 54000, Pakistan*
[b]*Institute of Semiconductor Physics, Univeristy of Linz, 4040 Linz, Austria*

Abstract

For the application of various theories to find a growth model for rubrene, it is essential to analyze the nucleation process during initial stages of growth. Here we present a study of rubrene deposited by Hot Wall Epitaxy on mica and SiO_2 using different substrate temperatures and calculating the island size distribution for each temperature. In order to find a growth model for rubrene we apply scaling theory during these initial stages of growth.

Keywords:
Nucleation, Scaling theory.

1. Introduction

Impressive new developments using organic materials has resulted in organic light emitting diodes (OLEDs) [1–4] as well as flexible devices [5] with the future being of organic solar cells [6, 7] and organic field effect transistors (OFETs) [8, 9]. However, the efficiency of any such device is compromised by the low charge carrier mobility. There needs to be intensive research into the charge transport system in crystalline form of organic materials [10–18] as well as the defining of models governing their growth. The attempt to predict the conditions of optimum growth of rubrene thin films on muscovite mica requires finding of a growth model for rubrene deposition. For this it is necessary to understand the nucleation process during the initial stages of island formation followed by application of different existing theories to the results. Here the scaling theory [19, 20], first shown by Venables et. al. [21], which has been successfully applied for formulating a growth model for pentacene [22] is selected and applied to rubrene during the initial stages of its growth.

2. Materials and Methods

An organic material called rubrene was acquired from Aldrich and subjected to thermal sublimation for additional purification. The substance was 98% pure. After being transferred into the Hot Wall Epitaxy device, Rubrene was put within a quartz tube. Acquired from Segliwa GMBH, $15 \times 15 mm^2$ Muscovite Mica substrates were manually split in the air prior to being put into the HWE vacuum chamber. Once a vacuum of 10-6 mbar was reached, the substrate deposition temperature was preheated for 15 minutes. With this in situ heat treatment, all materials that have adsorbed onto the substrate surface are completely eliminated. Rubrene was then applied on mica (001) and freshly cleaned SiO_2 wafer (SiO_2 coated Si wafer) substrates at a vacuum of 10-6 mbar. For mica, substrate temperatures of 90°C and 120°C were used, while for SiO_2, substrate temperatures of 120°C. In addition to the source temperature, the wall temperature was always kept at 180°C. The growth durations of the samples were 1, 2, 4, and 8 minutes. Making use of atomic force microscopy was utilized to perform morphological examinations on regions with dimensions of $10 \times 10 \mu m^2$ and $50 \times 50 \mu m^2$, using SiC tip. (AFM) images of the deposited organic thin films with a Digital Instruments Dimension 3100 microscope in the tapping mode. Fig. 1 shows these AFM pictures of rubrene applied to SiO_2 and muscovite mica surfaces. This series of AFM scans was subjected to the analysis that follows. One way to determine the island density would be to count the grains per $10 \times 10 \mu m^2$. After a large number of cross sections were analyzed, the average height of these islands was found. The distribution of island heights was then computed using this information.

*Corresponding Author:
aaliya.rehman@gmail.com (Aaliya Rehman)

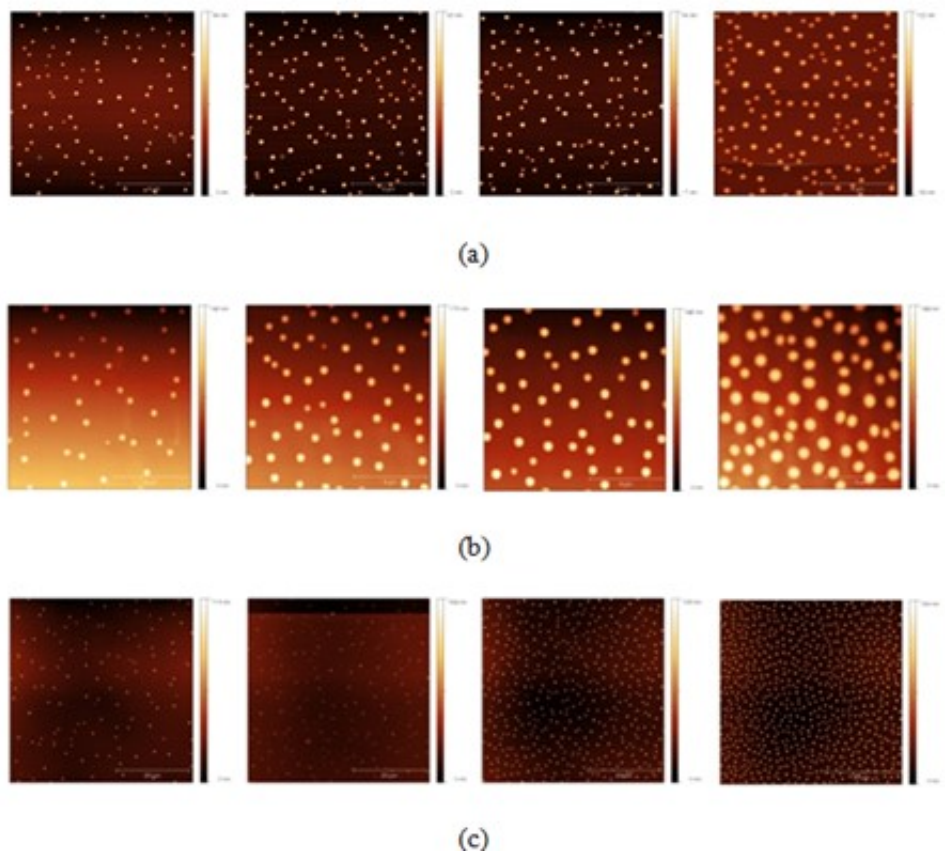

Figure 1. $10\times10\mu m^2$ AFM images of rubrene grown on mica for 1, 2, 4 and 8 minutes (left to right) at (a) T_{sub} = 90°C and (b) T_{sub} = 120°C and $50\times50\mu m^2$ AFM images of (c) SiO_2 for 0.5, 1, 2 and 4 minutes (left to right) at T_{sub} = 120°C.

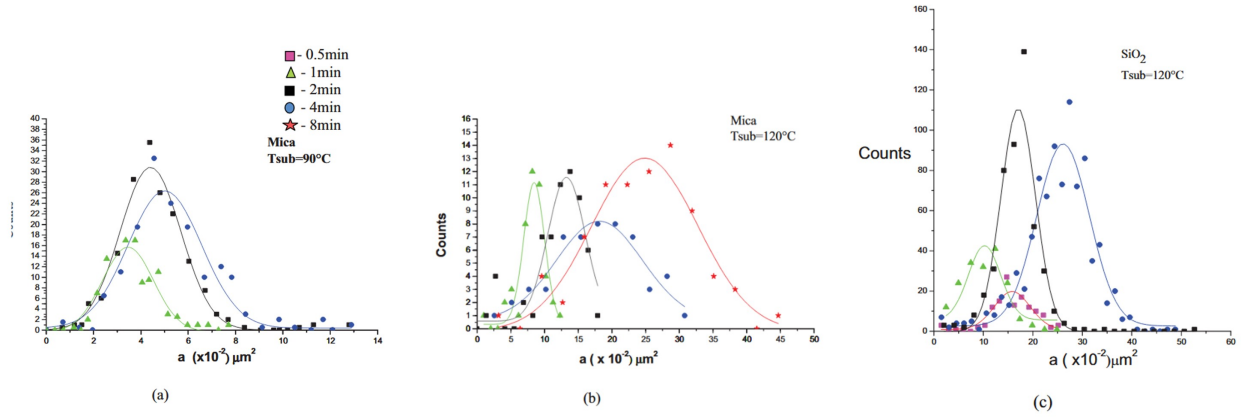

Figure 2. Island size distribution density for rubrene coverages of a few monolayers on mica at (a) T_{sub} = 90°C, (b) T_{sub} = 120°C and (c) SiO_2 at T_{sub} = 120°C.

3. Results and Discussion

The growth rate in the two series of samples was found by plotting the measured film thickness versus the time of growth and which gave the corresponding growth rate in monolayers (ML) per minute. The coverages for all three series of samples calculated from their growth rates ranged from less than a ML to around 4 ML´s. Hence the scaling theory which holds for the first few monolayers of growth, was applied to these samples. The island size distribution density is calculated from the AFM micrograph´s frequency count analysis and is plotted for the first few monolayers of rubrene growth in Fig. 2

We have used the scaling law here and apply it to the island size distribution density and observe that all the curves collapse into fi(u) where fi(u) is the scaling function and i is the critical nucleus size. A critical island size of 2 for T_{sub} = 90°C and about 30 for all other cases was obtained by the application of the rate equation and scaling theory. However, the question

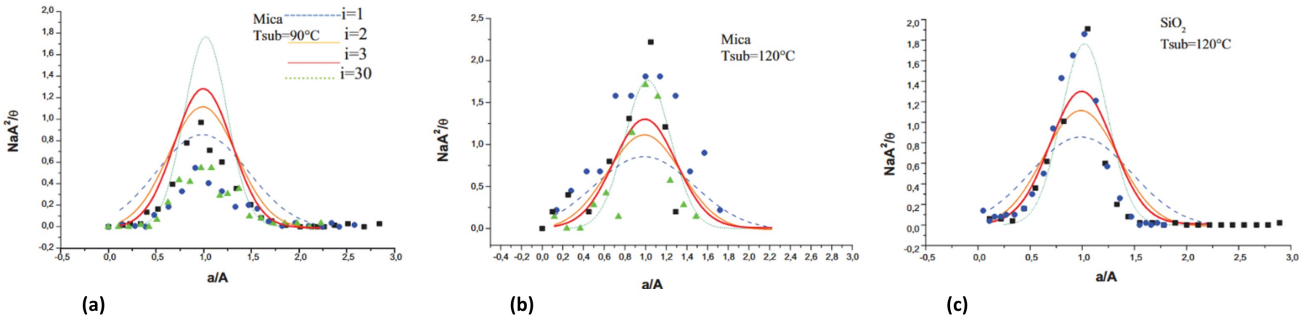

Figure 3. Scaled Island size distribution of rubrene grown on mica (a) T_{sub} = 90°C, (b) T_{sub} = 120°C and (c) SiO_2 at T_{sub} = 120°C.

remains whether this theory can explain the growth mechanism of rubrene if island heights reach many monolayers

4. Conclusion

We have presented the study of the nucleation stage of rubrene layers which were grown by Hot Wall Epitaxy (HWE) on two substrates at different temperatures. The plots show an agreement between model and data in cases of fig. 3b and 3c where fi(u) = 30. However, this seems too high a value for critical island size for rubrene. Although we restricted our investigations to the first few monolayers of rubrene, it is important to mention that the island heights were much more than that. Hence, we conclude that the scaling theory cannot be applied to the investigation of materials which have island heights exceeding the first few monolayers.

References

[1] C. W. Tang, S. A. VanSlyke, Organic electroluminescent diodes, Applied physics letters 51 (12) (1987) 913–915.
[2] M. Muccini, A bright future for organic field-effect transistors, Nature materials 5 (8) (2006) 605–613.
[3] S. Hirata, Y. Sakai, K. Masui, H. Tanaka, S. Y. Lee, H. Nomura, N. Nakamura, M. Yasumatsu, H. Nakanotani, Q. Zhang, et al., Highly efficient blue electroluminescence based on thermally activated delayed fluorescence, Nature materials 14 (3) (2015) 330–336.
[4] S. Scholz, D. Kondakov, B. Lussem, K. Leo, Degradation mechanisms and reactions in organic light-emitting devices, Chemical reviews 115 (16) (2015) 8449–8503.
[5] T. Someya, Z. Bao, G. G. Malliaras, The rise of plastic bioelectronics, Nature 540 (7633) (2016) 379–385.
[6] H. Sirringhaus, 25th anniversary article: organic field-effect transistors: the path beyond amorphous silicon, Advanced materials 26 (9) (2014) 1319–1335.
[7] B. Lussem, C.-M. Keum, D. Kasemann, B. Naab, Z. Bao, K. Leo, Doped organic transistors, Chemical reviews 116 (22) (2016) 13714–13751.
[8] A. J. Heeger, 25th anniversary article: bulk heterojunction solar cells: understanding the mechanism of operation, Advanced materials 26 (1) (2014) 10–28.
[9] R. A. Street, Electronic structure and properties of organic bulk-heterojunction interfaces, Advanced Materials 28 (20) (2016) 3814–3830.
[10] S. R. Forrest, The path to ubiquitous and low-cost organic electronic appliances on plastic, nature 428 (6986) (2004) 911–918.
[11] R. W. I. de Boer, M. Gershenson, A. Morpurgo, V. Podzorov, Organic single-crystal field-effect transistors, physica status solidi (a) 201 (6) (2004) 1302–1331.
[12] G. Malliaras, R. Friend, An organic electronics primer, Physics Today 58 (5) (2005) 53–58.
[13] H. Najafov, B. Lee, Q. Zhou, L. C. Feldman, Podzorov, V, Observation of long-range exciton diffusion in highly ordered organic semiconductors, Nature materials 9 (11) (2010) 938–943.
[14] I. G. Lezama, M. Nakano, N. A. Minder, Z. Chen, F. V. Di Girolamo, A. Facchetti, A. F. Morpurgo, Single-crystal organic charge-transfer interfaces probed using schottky-gated heterostructures, Nature materials 11 (9) (2012) 788–794.
[15] S. Z. Bisri, K. Sawabe, M. Imakawa, K. Maruyama, T. Yamao, S. Hotta, Y. Iwasa, T. Takenobu, Organic single-crystal light-emitting transistor coupling with optical feedback resonators, Scientific Reports 2 (1) (2012) 985.
[16] S. Illig, A. S. Eggeman, A. Troisi, L. Jiang, C. Warwick, M. Nikolka, G. Schweicher, S. G. Yeates, Y. Henri Geerts, J. E. Anthony, et al., Reducing dynamic disorder in small-molecule organic semiconductors by suppressing large-amplitude thermal motions, Nature communications 7 (1) (2016) 10736.
[17] M. Kikuchi, K. Takagi, H. Naito, M. Hiramoto, Single crystal organic photovoltaic cells using lateral electron transport, Organic Electronics 41 (2017) 118–121.
[18] X. Ren, M. J. Bruzek, D. A. Hanifi, A. Schulzetenberg, Y. Wu, C.-H. Kim, Z. Zhang, J. E. Johns, A. Salleo, S. Fratini, et al., Negative isotope effect on field-effect hole transport in fully substituted 13c-rubrene, Advanced Electronic Materials 3 (4) (2017) 1700018.
[19] R. Ruiz, B. Nickel, N. Koch, L. C. Feldman, R. F. Haglund Jr, A. Kahn, F. Family, G. Scoles, Dynamic scaling, island size distribution, and morphology in the aggregation regime of submonolayer pentacene films, Physical review letters 91 (13) (2003) 136102.
[20] J. G. Amar, F. Family, Critical cluster size: Island morphology and size distribution in submonolayer epitaxial growth, Physical Review Letters 74 (11) (1995) 2066.
[21] J. Venables, G. Spiller, M. Hanbucken, Nucleation and growth of thin films, Reports on progress in physics 47 (4) (1984) 399.
[22] B. Stadlober, U. Haas, H. Maresch, A. Haase, Growth model of pentacene on inorganic and organic dielectrics based on scaling and rate-equation theory, Physical Review B 74 (16) (2006) 165302.

RESEARCH PROSPECTS IN NATURAL SCIENCES IS A BIANNUAL SCHOLARLY PERIODICAL ISSUED BY GOVT GRADUATE COLLEGE TOWNSHIP, LAHORE, THAT STRIVES TO DISSEMINATE THE EMPIRICAL WORK OF RESEARCHERS WORLDWIDE THROUGH SCRUTINIZED RESEARCH ARTICLES, WITH THE INTENTION OF ESTABLISHING ITSELF AS A LEADING FORUM FOR TOP-NOTCH RESEARCH PUBLICATIONS AND ENDORSING LEARNED TREATISES AND RESEARCH PAPERS.

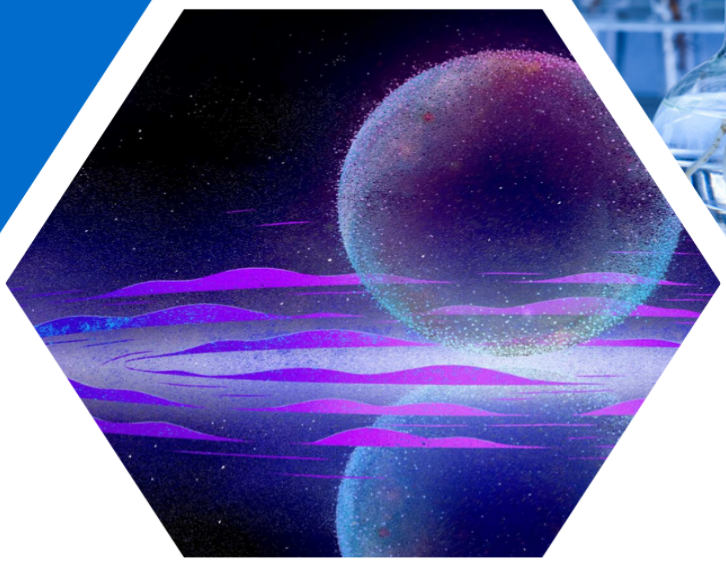

GOVERNMENT GRADUATE COLLEGE, TOWNSHIP, LAHORE